
Discovering Abstract Symbolic Relations by Learning Unitary Group Representations

Dongsung Huh

MIT-IBM Watson AI Lab, Cambridge MA, USA 02139
huh@ibm.com

Abstract

We investigate a principled approach for symbolic operation completion (SOC), a minimal task for studying symbolic reasoning. While conceptually similar to matrix completion, SOC poses a unique challenge in modeling abstract relationships between discrete symbols. We demonstrate that SOC can be efficiently solved by a minimal model — a bilinear map — with a novel factorized architecture. Inspired by group representation theory, this architecture leverages matrix embeddings of symbols, modeling each symbol as an operator that dynamically influences others. Our model achieves perfect test accuracy on SOC with comparable or superior sample efficiency to Transformer baselines across most datasets, while boasting significantly faster learning speeds (100~1000×). Crucially, the model exhibits an implicit bias towards learning general group structures, precisely discovering the unitary representations of underlying groups. This remarkable property not only confers interpretability but also significant implications for automatic symmetry discovery in geometric deep learning. Overall, our work establishes group theory as a powerful guiding principle for discovering abstract algebraic structures in deep learning, and showcases matrix representations as a compelling alternative to traditional vector embeddings for modeling symbolic relationships.

1 Introduction

Symbolic reasoning is fundamental to diverse areas such as knowledge representation, theorem proving, and natural language processing. While large-scale Transformer models show promise in tackling complex tasks within these domains, the complexity of the models and problem settings often obscures the underlying mechanisms. In this work, we adopt a minimalist approach, focusing on a simplified setting that enables detailed analysis of how models acquire and process symbolic relationships.

Symbolic operation completion (SOC) provides such a minimal setting, entailing the completion of "multiplication" tables of abstract symbols governed by binary operations (Figure 1). This focus on basic symbolic operations isolates a core aspect of symbolic reasoning: the ability to infer relationships between symbols based on their observed interactions. SOC shares conceptual similarities with matrix completion, which has been instrumental in exploring theoretical questions about generalization bounds, learnability, and implicit biases in deep learning. Likewise, SOC offers the potential to unveil the fundamental principles that govern symbolic reasoning.

We demonstrate that SOC can be effectively solved by a minimal model: a bilinear map. Inspired by group representation theory, we employ a novel architecture that leverages matrix embedding of symbols, and a regularizer that promotes learning general group structures — a principle akin to the low-rank bias used in matrix completion. The simplicity of this model and problem setting facilitates a thorough analysis, elucidating the core mechanisms underlying symbolic reasoning in SOC.

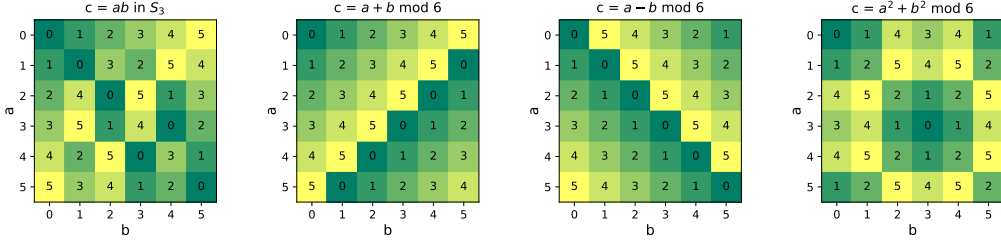


Figure 1: Small symbolic operation tables (Cayley tables): Symmetric (permutation) group S_3 , modular addition, subtraction, and squared addition. Elements of S_3 are illustrated in Figure 8.

2 Background

2.1 Low-rank Matrix Completion

Matrix completion, the task of recovering missing entries within a matrix, is a fundamental problem with broad applications in recommender systems, data imputation, compressed sensing, and signal processing. Classical approaches often rely on a low-rank structural assumption, achieved through explicit rank constraints (Burer and Monteiro, 2003) or by minimizing the nuclear norm as a convex surrogate for rank (Fazel et al., 2001; Candès and Recht, 2009; Recht et al., 2010; Candès and Tao, 2010). Recent works have demonstrated that deep matrix factorization, when regularized with L2 regularization or initialized with small weights, exhibit an implicit bias towards low-rank solutions (Srebro et al., 2004; Gunasekar et al., 2017). This implicit approach has demonstrated improved performance in matrix completion, particularly in the limited data regime (Arora et al., 2019).

2.2 Symbolic Operation Completion (SOC)

Power et al. (2022) introduced SOC as a simplified setting to investigate how deep learning models, particularly Transformers, acquire symbolic relationships from limited data. However, while Transformers could eventually solve the tasks with extensive hyperparameter tuning, they often struggled to generalize efficiently, requiring training times far exceeding those of simple memorization — a phenomenon termed *grokking*. Subsequent studies have further explored this phenomenon (Liu et al., 2022; Nanda et al., 2022; Chughtai et al., 2023).

These findings suggest that Transformers may lack the appropriate inductive biases for effectively discovering structures within abstract symbolic relationships, raising broader theoretical questions about the nature of these structures and the types of biases that facilitate their discovery. In this work, we leverage SOC as a testbed to address these questions.

3 Group Representation Theory

We briefly summarize group representation theory, providing key relevant concepts for our work.

Groups A group (G, \circ) is a set G with a binary operation \circ that satisfies the following axioms: Closure: $\forall a, b \in G, a \circ b \in G$. Associativity: $(a \circ b) \circ c = a \circ (b \circ c)$. Identity e : $g \circ e = e \circ g = g$, $\exists e, \forall g \in G$. Inverse: For every g , there exists a unique inverse g^{-1} such that $g \circ g^{-1} = g^{-1} \circ g = e$.

Representations A representation of a group (G, \circ) on a vector space V is a *group homomorphism* $\varrho: G \rightarrow GL(V)$ that preserves the group structure: *i.e.*

$$\varrho(g_1 \circ g_2) = \varrho(g_1)\varrho(g_2), \quad \forall g_1, g_2 \in G. \quad (1)$$

For a vector space of finite dimension n , we can choose a basis and identify $GL(V)$ with $GL(n, K)$, *i.e.* the group of $n \times n$ invertible matrices over the field K .

Equivalent Representations Given two vector spaces V and W , two representations $\varrho: G \rightarrow GL(V)$ and $\pi: G \rightarrow GL(W)$ are equivalent if there exists a vector space isomorphism $M: V \rightarrow W$, such that for all $g \in G$, $M\varrho(g)M^{-1} = \pi(g)$, *i.e.* a similarity transformation.

Unitary Representations A representation ρ of a group (G, \circ) is considered *unitary* if every matrix $\rho(g)$ is unitary for all $g \in G$. Crucially, the *Unitarity Theorem* guarantees that any finite-dimensional representation of a compact/finite group can be expressed as an equivalent unitary representation.

Irreducible Representations A representation is considered *reducible* if it can be decomposed into a direct sum of smaller representations via a similarity transform, which leads to a block-diagonal matrix form where each block corresponds to a simpler representation. *Irreducible* representations (*irreps*) serve as the fundamental building blocks for constructing all possible group representations.

Regular Representation Every group (G, \circ) possesses an inherent action on itself that can be viewed as a permutation, where each group element rearranges the other elements. The *regular* representation uses the permutation’s basis vectors to construct a linear representation. It is decomposable into a direct sum of the *complete* set of irreps, where each irrep appears with a multiplicity equal to its dimension. Moreover, its trace, also known as *character*, is a simple function:

$$\text{Tr } \rho(g) = n \text{ if } g = e \text{ else } 0. \quad (2)$$

Real vs Complex Representations Complex representations ($K = \mathbb{C}$) provide a rich mathematical framework for analyzing group structures in representation theory. We utilize this framework to establish the theoretical foundations of our approach in Sections 4 and 5. However, for finite groups, real representations ($K = \mathbb{R}$) often suffice in practice,¹ offering advantages in implementation and visualization. Our empirical results in Sections 6 and 7 thus utilize real representations.

4 Modeling Framework

Notations and Definitions We use the following capital symbols for order-3 tensor factors: A, B, C . A_a denotes the matrix slice of A at the first index a and A_a^\dagger denotes its conjugate transpose. $A_a B_b$ denotes the matrix product of A_a and B_b . Einstein convention is used, where repeated indices implies a contraction, *i.e.* summation over the index: *e.g.* $A_a A_a^\dagger \equiv \sum_a A_a A_a^\dagger$, unless noted otherwise.

4.1 Symbolic Operations as Bilinear Maps

Consider a binary operation $\circ : S \times S \rightarrow S$ over a finite set S containing n distinct symbols: *i.e.* $a \circ b = c$, where $a, b, c \in S$. To facilitate modeling, we linearize the problem by considering a homomorphism $\phi : (S, \circ) \rightarrow (V, \mathcal{D})$, where V is a vector space and $\mathcal{D} : V \times V \rightarrow V$ is a bilinear map over V , such that $\mathcal{D}(\phi(a), \phi(b)) = \phi(a \circ b)$. Specifically, we use the vector space $V = \mathbb{C}^n$ with a standard basis, *i.e.* encoding each symbol as a one-hot vector. In this framework, the bilinear map \mathcal{D} is represented by an order-3 tensor $D \in \mathbb{C}^{n \times n \times n}$, whose entries are

$$D_{abc} = \begin{cases} 1 & \text{if } a \circ b = c \\ 0 & \text{otherwise,} \end{cases}$$

where elements of S are used as indices of D for easy readability.

This framework shows that any binary operation over a finite set can be fully expressed as a tensor. Crucially, it transforms the problem of SOC into a tensor completion problem, where we recover the missing entries of D from the observed entries in the training set Ω_{train} .

4.2 HyperCube Parameterization

We consider a minimal end-to-end model, a bilinear map $\mathcal{T} : V \times V \rightarrow V$, to approximate \mathcal{D} . We introduce a novel architecture called *HyperCube*, which parameterizes the model tensor as a product of three order-3 factors $A, B, C \in \mathbb{C}^{n \times n \times n}$ (*i.e.* *cubes*. See Figure 2.):

$$T_{abc} = \frac{1}{n} \text{Tr}[A_a B_b C_c] = \frac{1}{n} \sum_{ijk} A_{aki} B_{bij} C_{cjk}. \quad (3)$$

¹For finite groups, every complex representation can be realized over the real numbers with a doubling of the dimension.

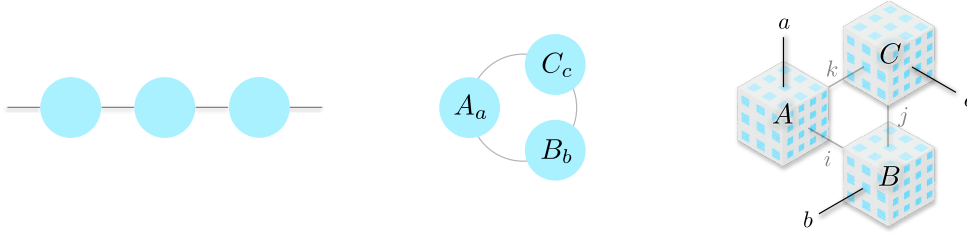


Figure 2: Visual illustration of matrix and tensor products. Nodes are factors and edges are indices. (Left) Matrix product. (Middle) Matrix product with trace operation. (Right) HyperCube product.

HyperCube can be viewed as a type of tensor decomposition,² but it crucially differs from existing decomposition methods, which often employ lower-order factors (e.g., vectors or matrices) to reduce model complexity. In contrast, HyperCube preserves the full expressive capacity of T without restricting the model’s hypothesis space.

More intuitively, HyperCube can be understood as modeling symbols and their interactions using matrix embeddings and multiplications: Factors A and B function as embedding dictionaries that map each symbol a and b to their respective matrix embeddings (A_a, B_b) . The model then calculates the interaction between a and b via matrix multiplication $(A_a B_b)$. Finally, factor C maps this result back to the space of symbols — *i.e.* the *unembedding* dictionary. Importantly, this (un)embedding process is directly related to the generalized (inverse) Fourier transform on groups. See Appendix E.

4.3 Regularization

The model is trained by minimizing the following regularized objective:

$$\mathcal{L} = \mathcal{L}_o(T; D) + \epsilon \mathcal{H}(A, B, C), \quad (4)$$

where \mathcal{H} is the HyperCube regularizer defined as

$$\mathcal{H} \equiv \frac{1}{n} \text{Tr} \left[A_a^\dagger A_a B_b B_b^\dagger + B_b^\dagger B_b C_c C_c^\dagger + C_c^\dagger C_c A_a A_a^\dagger \right]. \quad (5)$$

and \mathcal{L}_o is a differentiable loss on the end-to-end model, *e.g.* total squared error over Ω_{train}

$$\mathcal{L}_o(T; D) = \sum_{(a,b,c) \in \Omega_{\text{train}}} (T_{abc} - D_{abc})^2, \quad (6)$$

4.4 Internal Symmetry of Model

The redundant parameterization of eq (3) implies the existence of internal symmetry that leaves the model unchanged. For example, one can introduce arbitrary invertible matrices M_I, M_J, M_K and their inverses between the factors as $\tilde{A}_a = M_K^{-1} A_a M_I$, $\tilde{B}_b = M_I^{-1} B_b M_J$, and $\tilde{C}_c = M_J^{-1} C_c M_K$. These yield an equivalent parameterization of T , since $\text{Tr}[\tilde{A}_a \tilde{B}_b \tilde{C}_c] = \text{Tr}[A_a B_b C_c]$. These symmetry transformations can be understood as changing the internal basis coordinates.

Note that while the model loss $\mathcal{L}_o(T)$ is invariant under such coordinate changes, the regularizer $\mathcal{H}(A, B, C)$ is not. However, the regularizer is invariant under *unitary* basis changes, in which the introduced matrices are unitary U_I, U_J, U_K , such that $UU^\dagger = U^\dagger U = I$. Therefore, the regularizer imposes a stricter form of symmetry. This leads to the following Proposition.

Proposition 4.1. *If A, B, C form the optimal solution of the regularized loss eq (4), then any unitary basis changes leave the solution optimal, but non-unitary basis changes generally increase the loss.*

5 Analyzing HyperCube’s Inductive Bias

While HyperCube eq (3) does not explicitly restrict the model’s hypothesis space, the regularizer eq (5) induces a strong implicit bias that guides the model towards specific solutions. In this section, we introduce key concepts for analyzing this inductive bias. See Appendix C for proofs.

²It is closely related to the architecture used in tensor ring decomposition (Zhao et al., 2016).

Lemma 5.1 (Balanced Condition). *At stationary points of eq (4), imbalance terms vanish to zero:*

$$\xi_I = \xi_J = \xi_K = 0, \quad (7)$$

where $\xi_I = A_a^\dagger(C_c^\dagger C_c)A_a - B_b(C_c C_c^\dagger)B_b^\dagger$, $\xi_J = B_b^\dagger(A_a^\dagger A_a)B_b - C_c(A_a A_a^\dagger)C_c^\dagger$, and $\xi_K = C_c^\dagger(B_b^\dagger B_b)C_c - A_a(B_b B_b^\dagger)A_a^\dagger$ are the imbalances across edge i, j , and k , respectively.

The following statements demonstrate that the regularizer promotes a unitarity condition.

Definition 5.2 (Contracted Unitarity). A factor A is C -unitary if it satisfies the following: $A_a A_a^\dagger, A_a^\dagger A_a \propto I$ (with contracting the repeated index a).

Proposition 5.3. C -unitary factors satisfy the balanced condition eq (7), given that they share a common scalar multiple of the identity matrix: i.e.

$$A_a A_a^\dagger = A_a^\dagger A_a = B_b B_b^\dagger = B_b^\dagger B_b = C_c C_c^\dagger = C_c^\dagger C_c \equiv n\alpha^2 I, \quad (8)$$

Lemma 5.4. Under the fixed Frobenius norm, all C -unitary factors are stationary points of the regularizer \mathcal{H} .

Lemma 5.4 indicates that \mathcal{H} effectively promotes C -unitarity as well as minimizing the Frobenius norm. Remarkably, we also observe a stronger form of unitarity in the converged solutions.

Definition 5.5 (Slice Unitarity). A factor A is S -unitary if every matrix slice of A is a scalar multiple of a unitary matrix: i.e. $A_a A_a^\dagger = A_a^\dagger A_a \equiv \alpha_{A_a}^2 I$ (without contracting the repeated index a).

Observation 5.6. When optimizing the regularized loss eq (4), C -unitary solutions are consistently achieved via S -unitarity, in which eq (8) reduces to $\sum_a \alpha_{A_a}^2 = \sum_b \alpha_{B_b}^2 = \sum_c \alpha_{C_c}^2 = n\alpha^2$.

Although the exact mechanism driving S -unitarity remains an open question, this observation highlights the strong inductive bias towards unitarity imposed by the HyperCube regularizer.

6 Representation Learning in HyperCube

6.1 Learning Dynamics on partially observed S_3

We begin our analysis by examining how our model learns the symmetric group S_3 (using 60% of Cayley table as training data). Figure 4 visualizes the optimization trajectories under different regularization strategies, while Figure 3 depicts the resulting end-to-end model. The evolution of the model and its parameters is directly visualized in Figure 9. See Appendix A for training details.

In the absence of regularization, the model quickly memorizes the training dataset, achieving perfect training accuracy, but fails to generalize to the test dataset. Also, the singular values of the unfolded factors remain largely unchanged during training, indicating minimal internal structural changes.

Under HyperCube (\mathcal{H}) regularization, the model continues to improve on the test set even after perfect training accuracy is achieved. A critical turning point is observed around $t = 200$, marked by a sudden collapse of the singular values towards a common value, signifying convergence to a unitary solution. Concurrently, the C/S -unitarity and imbalance measures rapidly decrease to zero. This internal restructuring coincides with a substantial improvement in test performance, ultimately achieving 100% test accuracy, thus highlighting its crucial role in enabling generalization. Notably, when the regularization coefficient drops to 0 around $t = 450$, both the train and test losses plummet to 0, confirming perfect completion of D .

In contrast, L2 regularization drives the model towards a low-rank solution, as evidenced by a portion of its singular values decaying to zero. Although this training scheme shows some degree of generalization, it fails to reduce the test loss to zero, indicating imperfect recovery. On the modular addition task (Figure 12,13), L2-regularized training only achieves $\sim 50\%$ test accuracy. Figure 3 visually confirms these findings, demonstrating that only \mathcal{H} -regularized training is capable of accurately recovering D .

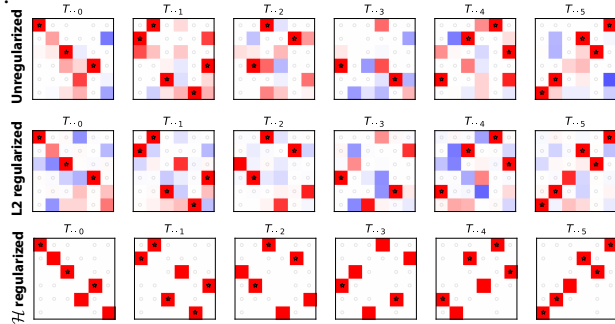


Figure 3: Model slices $T_{..c}$ after trained on the S_3 dataset. Training data are marked by stars (1s) and circles (0s).

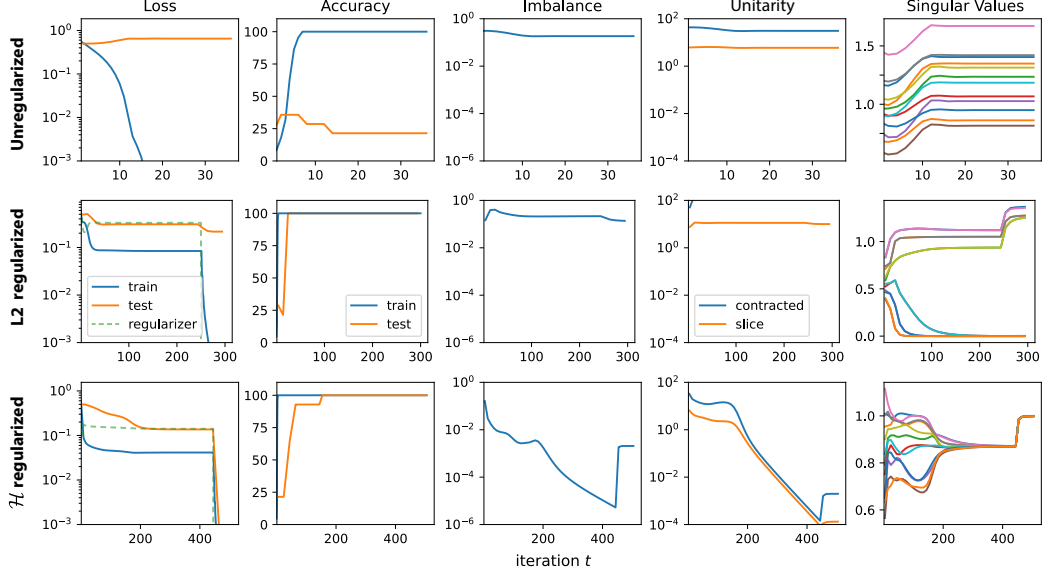


Figure 4: Optimization trajectories on the S_3 dataset with 60% training data fraction. (Top) Unregularized, (Middle) L2-regularized, and (Bottom) \mathcal{H} -regularized training. Column 3 shows the average imbalance $(\|\xi_I\|_F^2 + \|\xi_J\|_F^2 + \|\xi_K\|_F^2)^{1/2}$, and column 4 shows deviation from C-unitarity $\|\sum_a A_a A_a^\dagger/n - \alpha^2 I\|_F^2$ and S-unitarity $\|A_a A_a^\dagger - \alpha_{A_a}^2 I\|_F^2$, averaged over all factors and slices. Column 5 shows normalized singular values of unfolded factors A, B, C .

6.2 Model Learns Unitary Group Representations

In Figure 10, we analyze the learned factors in different basis coordinate representations, demonstrating a remarkable finding: The factors directly encode group representations.

(Top panel) In the raw basis coordinate, the factors exhibit unitary matrix slices, but no other easily identifiable structure.

(Middle panel) A unitary change of basis, such that the factor slices for the identity element become the identity matrix ($A_e = B_e = C_e = I$), reveals a surprising underlying structure:

- All factors share the same embedding, *i.e.* A_g equals B_g equals C_g^\dagger for all elements g .
- The factor slices satisfy *group homomorphism* eq (1): *i.e.* $A_{g_1} A_{g_2} = A_{g_1 \circ g_2}$. See Figure 11.
- Therefore, the factors form a unitary matrix representation ϱ of the group, where

$$A_g = B_g = C_g^\dagger = \varrho(g). \quad (9)$$

- Furthermore, the trace of factor slices satisfy eq (2), indicating that ϱ is a regular representation.

(Bottom panel) In a block-diagonalizing basis coordinate, the factors reveal the *complete set of irreps* contained in the regular representation ϱ , including the trivial (1-dim), sign (1-dim), and duplicate standard representations (2-dim), which form the generalized Fourier basis for group convolution.

Shared-Embedding Eq (9) reveals that, for group operations, the same embedding is used across all symbol positions. This motivates tying the embeddings across factors, resulting in a parameter-efficient model specifically tailored for learning group operations: HyperCube-SE (shared embedding).

Key Operating Mechanism Above results reveal the key mechanism by which HyperCube operates on groups. According to eq (9) and the homomorphism property of ϱ , the model eq (3) can be expressed as

$$T_{abc} = \frac{1}{n} \text{Tr}[\varrho(a)\varrho(b)\varrho(c)^\dagger] = \frac{1}{n} \text{Tr}[\varrho(a \circ b \circ c^{-1})]. \quad (10)$$

Since $a \circ b = c$ is equivalent to $a \circ b \circ c^{-1} = e$, applying eq (2) implies that $T_{abc} = D_{abc}$. Notably, this mechanism applies universally for all finite groups, yielding exact one-hot encoding for the output symbols. This insight leads us to the following conjecture:

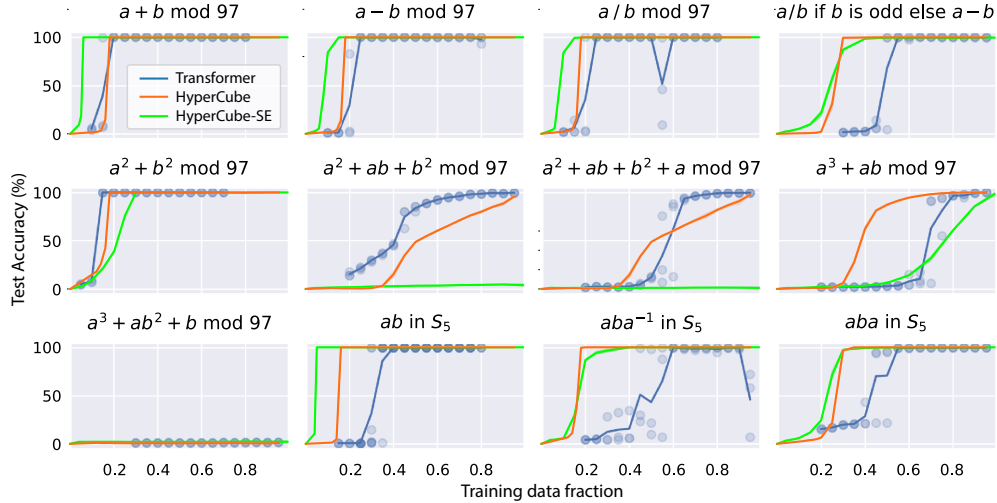


Figure 5: Generalization performance (test accuracy) shown as a function of training data fraction across a diverse set of symbolic operation tasks. Trial-to-trial variation due to randomized model initialization and data split is shown as dots for Transformer and as shaded area for HyperCubes.

Conjecture 6.1. Let D represent a group operation table. Then, given the constraint $T = D$, the unitary group representation eq (9) describes the unique minimizer of HyperCube Regularizer eq (5) up to unitary basis changes, whose minimum regularizer loss is $\mathcal{H}^*(D) = 3\|D\|_F^2$.

6.3 Discovering Unitary Representations Beyond True Groups

We trained HyperCube on the remaining small operation tasks from Figure 1. Interestingly, the model learns closely related representations across these tasks (See Figure 14).

Modular addition ($a + b$) forms the cyclic group C_6 . As expected, HyperCube learns the regular representation $\varrho(g)$ of C_6 in its factors, as described by eq (9).

Modular Subtraction ($a - b$) violates associativity and therefore isn't a true group. Surprisingly, HyperCube still learns the same representation as addition but with transposed factors: $A_g^\dagger = B_g = C_g = \varrho(g)$. This reflects the equivalence: $a - b = c \Leftrightarrow a = b + c$.

Modular Squared Addition ($a^2 + b^2$) violates the inverse axiom. Still, HyperCube learns the same representation as addition for elements with unique inverses (e.g., 0, 3). For others, it learns *duplicate* representations reflecting the periodicity of squaring modulo: e.g., $A_2 = A_4$ since $2^2 = 4^2 \pmod{6}$.

These results highlight the remarkable flexibility of HyperCube's inductive bias: Even for *group-like* operations (i.e., those deviating from strict group axioms), HyperCube often discovers meaningful unitary representations. This finding highlights the potential of unitary representations as a powerful tool for understanding symbolic operations beyond the confines of strict group theory.

7 Results on Diverse SOC Datasets

We trained HyperCube and HyperCube-SE on diverse SOC datasets from Power et al. (2022), encompassing various group and non-group operations (details in Appendix B). These problems are significantly larger than our previous examples, with dimensions ranging from $n = 97$ to 120. Figure 5 compares their performance to the baseline Transformer results from Power et al. (2022).

HyperCube demonstrates remarkable generalization across a wide range of tasks. On *simpler* tasks, it achieves perfect test accuracy with only $\sim 18\%$ of the data, including group and *group-like* operations (Sec. 6.3) with known unitary representations, as well as group conjugation ($a \circ b \circ a^{-1}$ in S_5), which lack such representations. For more *complex* tasks, HyperCube requires more data for effective generalization, such as modular polynomials, conditional operations, and $a \circ b \circ a$ in S_5 . Overall,

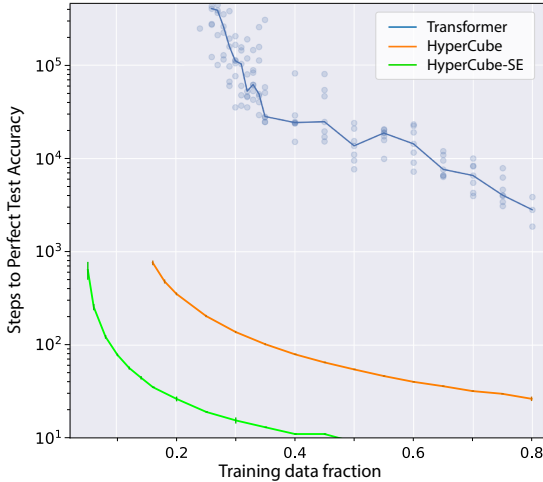


Figure 6: Training steps to achieve perfect test accuracy on the $(ab \text{ in } S_5)$ task.

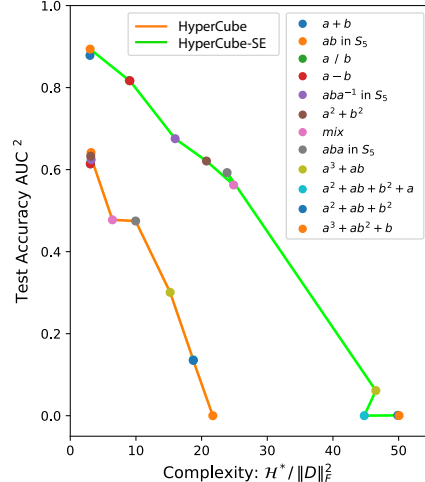


Figure 7: Complexity vs Generalizability. (AUC \equiv Area Under the Curve)

Hypercube exhibits comparable or superior generalizability to the Transformer baseline on all but two tasks (modular $a^2 + ab + b^2$ and $a^2 + ab + b^2 + a$).

HyperCube-SE demonstrates a similar trend but with a narrower inductive bias towards group operations. It requires even less data for group operations but shows weaker generalization on non-group operations, especially high-order modular polynomials.

Blazing-Fast Learning Beyond its sample efficiency, HyperCube exhibits exceptional learning speed. As shown in Figure 6 on the S_5 group operation, it converges to perfect test accuracy 100 times faster than the Transformer baseline, while requiring less data. HyperCube-SE, with shared factor weights ($A_g = B_g = C_g^\dagger$), similar to shared embeddings in Transformers, achieves an additional $10\times$ speedup and requires only 5% of the data for perfect generalization. This dramatic $1000\times$ improvement in learning speed demonstrates the effectiveness of our models’ inductive bias.

Complexity vs Generalizability In matrix factorization, the minimum L2 regularization loss implicitly defines a *complexity metric* that approximate rank: *e.g.*, nuclear or Schatten norm (Srebro et al., 2004). Similarly, we formally define a complexity metric for SOC as the minimum HyperCube regularization \mathcal{H}^* required to fit the full operation table. This metric aligns with the intuitive notion of complexity in symbolic operations (Figure 7). Group operations achieve the minimum complexity $\mathcal{H}^* = 3\|D\|_F^2$, indicating their inherent simplicity within HyperCube. *Group-like* operations also achieve this minimum in HyperCube but incur increased complexity in HyperCube-SE, demonstrating the latter’s narrower inductive bias towards pure group structures. In contrast, more complex tasks, such as modular polynomials, incur substantially higher complexity costs, culminating in the unsolvable cubic operation (modular $a^3 + ab^2 + b$).

Figure 7 illustrates the generalization trends as a function of complexity, revealing a clear monotonic relationship: increasingly complex tasks exhibit lower generalizability (measured as the total area under the test accuracy curve). This observation underscores the critical role of our proposed complexity metric in determining the generalization bound for SOC, mirroring the relationship between matrix rank, observed entries, and generalization error in matrix completion.

8 Conclusion

In this work, we investigated symbolic operation completion (SOC) as a minimal yet fundamental task for studying symbolic reasoning. We demonstrated that these tasks can be effectively solved using a simple bilinear model with a factorized architecture, and revealed the key principles underlying symbolic reasoning in SOC by analyzing the model.

Our core innovation lies in representing symbols and their interactions via matrix embeddings and matrix multiplications, modeling each symbol as an operator that dynamically influences others. This operator-based approach³ aligns with the principles of *dynamic semantics* in linguistics, where words are seen as context-changing operators (Kamp, 1981; Heim, 1982). It also resonates with earlier explorations of compositional representations in connectionist models (Smolensky, 1990) and recursive neural networks (Socher et al., 2012). This contrasts with traditional vector embeddings (e.g., word embeddings), which primarily capture static semantic meaning and necessitate additional mechanisms to model interactions between symbols (e.g., self-attention in Transformers).

While deep learning models have previously utilized multiplicative interactions for specific purposes, such as fusing information from multiple inputs or mediating context-dependent computations (e.g., in FiLM layers, gating mechanisms, and Hypernetworks), these applications have been relatively limited in scope (Jayakumar et al., 2020). Our work expands the role of multiplicative interactions, demonstrating their effectiveness as the primary computational primitive for modeling abstract relationships between multiple input elements.

Another core contribution is our novel regularizer, which unlocks the full potential of matrix embeddings. By implicitly promoting unitary representations, this regularizer instills a powerful inductive bias towards discovering general group structures in data. This bias, akin to the low-rank bias in matrix completion, provides a novel way to quantify the simplicity of symbolic operations, and offers an effective solution for inferring symbolic relationships from limited observations.

Symmetry Discovery The bias towards general groups offers a promising new paradigm for leveraging symmetries in deep learning. Current approaches often rely on manually designing architectures tailored to specific symmetry groups, such as equivariant networks (Bronstein et al., 2021). In contrast, our findings suggest a universal inductive bias towards the fundamental algebraic structures of groups, not specific symmetries, potentially enabling the discovery of symmetries across diverse domains without the need for bespoke architectures. Notably, the learned representations in HyperCube correspond to the generalized Fourier basis, which mediates the group convolution operation central to equivariant neural networks (see Appendix E). This connection positions HyperCube as a potential framework for automatically constructing symmetry-aware architectures directly from data.

Limitation While our method exhibits strong sample efficiency, the use of tensor factors can incur substantial memory and computational loads, scaling as $O(n^3)$. Potential mitigations include exploiting sparsity in the factors (e.g., block-diagonalization) or utilizing faithful representations of smaller dimensions ($d \times d, d \ll n$). Even though such representations do not strictly adhere to eq (2), they can still yield correct predictions for the Cayley tables, since they satisfy eq (10) and the maximum value of their characters is achieved by the identity element: *i.e.* $\operatorname{argmax} \operatorname{Tr}[\rho(g)] = e$.

Open Questions This work leaves several open questions for future studies, such as deriving exact generalization bounds for SOC. Additionally, proving Observation 5.6 and Conjecture 6.1 on the optimality of unitary representations remains an open challenge. Furthermore, scaling the method to problems involving multiple symbols beyond binary operations is an important direction for future research.

In summary, our work establishes group theory as a powerful guiding principle for discovering abstract algebraic structures in deep learning, and showcases matrix representations as a compelling alternative to traditional vector embeddings for modeling symbolic relationships.

References

- Arora, S., Cohen, N., Hu, W., and Luo, Y. (2019). Implicit Regularization in Deep Matrix Factorization. arXiv:1905.13655 [cs, stat].
- Bronstein, M. M., Bruna, J., Cohen, T., and Veličković, P. (2021). Geometric Deep Learning: Grids, Groups, Graphs, Geodesics, and Gauges. arXiv:2104.13478 [cs, stat].
- Burer, S. and Monteiro, R. D. (2003). A nonlinear programming algorithm for solving semidefinite programs via low-rank factorization. *Mathematical Programming*, 95(2):329–357.

³The operator-based perspective is also fundamental in quantum mechanics, where unitary matrix operators describe how physical systems evolve over time.

- Candes, E. J. and Tao, T. (2010). The Power of Convex Relaxation: Near-Optimal Matrix Completion. *IEEE Transactions on Information Theory*, 56(5):2053–2080.
- Candès, E. J. and Recht, B. (2009). Exact Matrix Completion via Convex Optimization. *Foundations of Computational Mathematics*, 9(6):717–772.
- Chughtai, B., Chan, L., and Nanda, N. (2023). Neural Networks Learn Representation Theory: Reverse Engineering how Networks Perform Group Operations. In *ICLR 2023 Workshop on Physics for Machine Learning*.
- Fazel, M., Hindi, H., and Boyd, S. (2001). A rank minimization heuristic with application to minimum order system approximation. In *Proceedings of the 2001 American Control Conference. (Cat. No.01CH37148)*, volume 6, pages 4734–4739 vol.6. ISSN: 0743-1619.
- Gunasekar, S., Woodworth, B. E., Bhojanapalli, S., Neyshabur, B., and Srebro, N. (2017). Implicit Regularization in Matrix Factorization. In *Advances in Neural Information Processing Systems*, volume 30. Curran Associates, Inc.
- Heim, I. R. (1982). The Semantics of Definite and Indefinite Noun Phrases. *Doctoral Dissertations Available from Proquest*, pages 1–426.
- Jayakumar, S. M., Czarnecki, W. M., Menick, J., Schwarz, J., Rae, J., Osindero, S., Teh, Y. W., Harley, T., and Pascanu, R. (2020). Multiplicative Interactions and Where to Find Them.
- Kamp, H. (1981). A Theory of Truth and Semantic Representation. In *Meaning and the Dynamics of Interpretation*, pages 329–369. Brill. Section: Meaning and the Dynamics of Interpretation.
- Liu, Z., Kitouni, O., Nolte, N., Michaud, E. J., Tegmark, M., and Williams, M. (2022). Towards Understanding Grokking: An Effective Theory of Representation Learning. In *Advances in Neural Information Processing Systems*.
- Nanda, N., Chan, L., Lieberum, T., Smith, J., and Steinhardt, J. (2022). Progress measures for grokking via mechanistic interpretability. In *The Eleventh International Conference on Learning Representations*.
- Power, A., Burda, Y., Edwards, H., Babuschkin, I., and Misra, V. (2022). Grokking: Generalization Beyond Overfitting on Small Algorithmic Datasets.
- Recht, B., Fazel, M., and Parrilo, P. A. (2010). Guaranteed Minimum-Rank Solutions of Linear Matrix Equations via Nuclear Norm Minimization. *SIAM Review*, 52(3):471–501.
- Smolensky, P. (1990). Tensor Product Variable Binding and the Representation of Symbolic Structures in Connectionist Systems. *Artificial Intelligence*, 46:159–216.
- Socher, R., Huval, B., Manning, C. D., and Ng, A. Y. (2012). Semantic Compositionality through Recursive Matrix-Vector Spaces. In Tsujii, J., Henderson, J., and Paşca, M., editors, *Proceedings of the 2012 Joint Conference on Empirical Methods in Natural Language Processing and Computational Natural Language Learning*, pages 1201–1211, Jeju Island, Korea. Association for Computational Linguistics.
- Srebro, N., Rennie, J., and Jaakkola, T. (2004). Maximum-Margin Matrix Factorization. In *Advances in Neural Information Processing Systems*, volume 17. MIT Press.
- Zhao, Q., Zhou, G., Xie, S., Zhang, L., and Cichocki, A. (2016). Tensor Ring Decomposition. arXiv:1606.05535 [cs].

A Training Procedure

The factor tensors are initialized with entries randomly drawn from a normal distribution with mean 0 and standard deviation $1/\sqrt{n}$. Real parameterization ($K = \mathbb{R}$) is used. We employ full-batch gradient descent to optimize the regularized loss with learning rate of 0.5 and momentum of 0.5. For the small scale experiments in Section 6, the HyperCube regularizer coefficient is set to $\epsilon = 0.1$. For the larger scale experiments in Section 7, we use $\epsilon = 0.05$ for HyperCube and $\epsilon = 0.01$ for HyperCube-SE. Each experiment can be quickly run within a few minutes on a single GPU machine.

ϵ -scheduler To overcome the limitations in standard regularized optimization, which often prevents full convergence to the ground truth (D), we employ ϵ -scheduler: Once the model demonstrates sufficient convergence (*e.g.* the average imbalance falls below a threshold of 10^{-5}), the scheduler sets the regularization coefficient ϵ to 0. This allows the model to fully fit the training data. The effect of ϵ -scheduler on convergence is discussed in Appendix C.3. Note that ϵ -scheduler only affects the overall scale of model’s output vector and does not affect the accuracy of output.

B List of Binary Operations

Here is the list of binary operations from Power et al. (2022) that are used in Section 7 (with $p = 97$).

- (add) $a \circ b = a + b \pmod{p}$ for $0 \leq a, b < p$. (Group operation)
- (sub) $a \circ b = a - b \pmod{p}$ for $0 \leq a, b < p$.
- (div) $a \circ b = a/b \pmod{p}$ for $0 \leq a < p, 0 < b < p$.
- (mix) $a \circ b = [a/b \pmod{p}$ if b is odd, otherwise $a - b \pmod{p}]$ for $0 \leq a, b < p$.
- (quad1) $a \circ b = a^2 + b^2 \pmod{p}$ for $0 \leq a, b < p$.
- (quad2) $a \circ b = a^2 + ab + b^2 \pmod{p}$ for $0 \leq a, b < p$.
- (quad3) $a \circ b = a^2 + ab + b^2 + a \pmod{p}$ for $0 \leq a, b < p$.
- (cube1) $a \circ b = a^3 + ab \pmod{p}$ for $0 \leq a, b < p$.
- (cube2) $a \circ b = a^3 + ab^2 + b \pmod{p}$ for $0 \leq a, b < p$.
- (ab in S_5) $a \circ b = a \cdot b$ for $a, b \in S_5$. (Group operation)
- (aba^{-1} in S_5) $a \circ b = a \cdot b \cdot a^{-1}$ for $a, b \in S_5$.
- (aba in S_5) $a \circ b = a \cdot b \cdot a$ for $a, b \in S_5$.

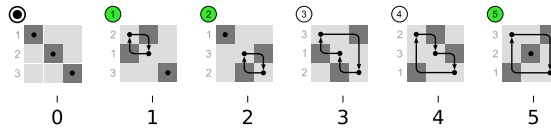


Figure 8: Elements of the symmetric group S_3 illustrated as permutations of 3 items. Green color indicates *odd* permutations, and white indicates *even* permutations. Adapted from https://en.wikipedia.org/wiki/Symmetric_group.

C Deferred Proofs

C.1 Proof of Lemma 5.1 on Balanced Condition

Here, we derive the balanced condition eq (7) in detail. First, we compute the gradient of the regularized loss $\mathcal{L} = \mathcal{L}_o(T) + \epsilon\mathcal{H}(A, B, C)$ eq (4),

$$\begin{aligned}\nabla_{A_a}\mathcal{L} &= \frac{1}{n}((\nabla_{T_{abc}}\mathcal{L}_o)C_c^\dagger B_b^\dagger + 2\epsilon(A_a(B_b B_b^\dagger) + (C_c^\dagger C_c)A_a)), \\ \nabla_{B_b}\mathcal{L} &= \frac{1}{n}((\nabla_{T_{abc}}\mathcal{L}_o)A_a^\dagger C_c^\dagger + 2\epsilon(B_b(C_c C_c^\dagger) + (A_a^\dagger A_a)B_b)), \\ \nabla_{C_c}\mathcal{L} &= \frac{1}{n}((\nabla_{T_{abc}}\mathcal{L}_o)B_b^\dagger A_a^\dagger + 2\epsilon(C_c(A_a A_a^\dagger) + (B_b^\dagger B_b)C_c)),\end{aligned}\tag{11}$$

where $\nabla_{A_a}\mathcal{L} \equiv \partial\mathcal{L}/\partial A_a$, $\nabla_{B_b}\mathcal{L} \equiv \partial\mathcal{L}/\partial B_b$, $\nabla_{C_c}\mathcal{L} \equiv \partial\mathcal{L}/\partial C_c$, and $\nabla_{T_{abc}}\mathcal{L}_o \equiv \partial\mathcal{L}_o/\partial T_{abc}$.

The *imbalances* in Lemma 5.1 are defined as the difference of loss gradient:

$$\begin{aligned}\xi_I &\equiv \frac{n}{2\epsilon}(A_a^\dagger(\nabla_a\mathcal{L}) - (\nabla_b\mathcal{L})B_b^\dagger) = A_a^\dagger(C_c^\dagger C_c)A_a - B_b(C_c C_c^\dagger)B_b^\dagger \\ \xi_J &\equiv \frac{n}{2\epsilon}(B_b^\dagger(\nabla_b\mathcal{L}) - (\nabla_c\mathcal{L})C_c^\dagger) = B_b^\dagger(A_a^\dagger A_a)B_b - C_c(A_a A_a^\dagger)C_c^\dagger \\ \xi_K &\equiv \frac{n}{2\epsilon}(C_c^\dagger(\nabla_c\mathcal{L}) - (\nabla_a\mathcal{L})A_a^\dagger) = C_c^\dagger(B_b^\dagger B_b)C_c - A_a(B_b B_b^\dagger)A_a^\dagger\end{aligned}$$

At stationary points, *i.e.* $\nabla_{A_a}\mathcal{L} = \nabla_{B_b}\mathcal{L} = \nabla_{C_c}\mathcal{L} = 0$, imbalance terms vanish to zero, yielding the balanced condition $\xi_I = \xi_J = \xi_K = 0$, which proves Lemma 5.1. Note that imbalance terms are defined to cancel out the $\nabla_{T_{abc}}\mathcal{L}_o$ terms. Therefore, the balanced condition is independent of the loss function \mathcal{L}_o .

C.2 Proof of Lemma 5.4

Proof. The constraint on Frobenius norm can be integrated with the regularizer into an augmented loss via the Lagrange multiplier λ

$$\mathcal{H} + \lambda(\mathcal{F} - \text{constant}),\tag{12}$$

where $\mathcal{F} \equiv \frac{1}{n} \text{Tr} [A_a^\dagger A_a + B_b^\dagger B_b + C_c^\dagger C_c]$ is the Frobenius norm .

The gradient of eq (12) with respect to A_a is proportional to

$$\nabla_{A_a}(\mathcal{H} + \lambda\mathcal{F}) \propto A_a(B_b B_b^\dagger) + (C_c^\dagger C_c)A_a + \lambda A_a.\tag{13}$$

In the case of C-unitary factors B and C , all terms in eq (13) become aligned to A_a , *i.e.*

$$\nabla_{A_a}(\mathcal{H} + \lambda\mathcal{F}) \propto (\alpha_B^2 + \alpha_C^2 + \lambda)A_a.\tag{14}$$

and thus an appropriate value for the Lagrange multiplier λ can be found to vanish the gradient, which confirms stationarity. This result also applies to gradient with respect to B_b and C_c by the symmetry of parameterization. \square

C.3 Persistence of Group Representation

The following lemma demonstrates a key property of our model's convergence behavior: once a group representation is learned, the solution remains within this representational form throughout optimization.

Lemma C.1. *Let D represent a group operation table. Once gradient descent of the regularized loss eq (4) converges to a group representation (including scalar multiples), *i.e.**

$$A_a = \alpha_{A_a}\varrho(a), B_b = \alpha_{B_b}\varrho(b), C_c = \alpha_{C_c}\varrho(c)^\dagger,\tag{15}$$

the solution remains within this representation form.

Proof. With the squared loss eq (6), the gradient with respect to A_a eq (11) becomes

$$\nabla_{A_a} \mathcal{L} = \frac{1}{n} (\Delta_{abc} M_{abc} C_c^\dagger B_b^\dagger + \epsilon (A_a (B_b B_b^\dagger) + (C_c^\dagger C_c) A_a)) \quad (16)$$

where $\Delta \equiv T - D$ is the constraint error, and M is the mask indicating observed entries in the train set.

Substituting the group representation form eq (15) into eq (16), we get:

$$\frac{1}{n} \epsilon (A_a (B_b B_b^\dagger) + (C_c^\dagger C_c) A_a) = 2\epsilon \alpha_{A_a} \alpha^2 \varrho(a), \quad (17)$$

for the last two terms, where $\alpha^2 = \sum_b \alpha_{B_b}^2 / n = \sum_c \alpha_{C_c}^2 / n$.

Since the product tensor is

$$T_{abc} = \frac{1}{n} \text{Tr}[A_a B_b C_c] = \frac{1}{n} \alpha_{A_a} \alpha_{B_b} \alpha_{C_c} \text{Tr}[\varrho(a) \varrho(b) \varrho(c)^\dagger] = \alpha_{A_a} \alpha_{B_b} \alpha_{C_c} D_{abc},$$

and $D_{abc} = \delta_{a \circ b, c} = \delta_{a, c \circ b^{-1}}$ (δ is the Kronecker delta function), the first term in eq (16) becomes

$$\begin{aligned} \frac{1}{n} \sum_{b,c} \Delta_{abc} M_{abc} C_c^\dagger B_b^\dagger &= \frac{1}{n} \sum_{b,c} \delta_{a \circ b, c} M_{abc} (\alpha_{A_a} \alpha_{B_b} \alpha_{C_c} - 1) \alpha_{B_b} \alpha_{C_c} \varrho(c \circ b^{-1}) \\ &= \frac{1}{n} \sum_b M_{ab(a \circ b)} (\alpha_{A_a} \alpha_{B_b} \alpha_{C_{a \circ b}} - 1) \alpha_{B_b} \alpha_{C_{a \circ b}} \varrho(a). \end{aligned} \quad (18)$$

Note that both eq (18) and eq (17) are proportional to $\varrho(a)$. Consequently, we have $\nabla_{A_a} \mathcal{L} \propto \varrho(a)$. Similar results for other factors can also be derived: $\nabla_{B_b} \mathcal{L} \propto \varrho(b)$, and $\nabla_{C_c} \mathcal{L} \propto \varrho(c)^\dagger$. This implies that gradient descent preserves the form of the group representation (eq (15)), only updating the coefficients $\alpha_{A_a}, \alpha_{B_b}, \alpha_{C_c}$. \square

Effect of ϵ -Scheduler Lemma C.1 holds true even when ϵ gets modified by ϵ -scheduler, which reduces ϵ to 0. In this case, the coefficients converge to $\alpha_{A_a} = \alpha_{B_b} = \alpha_{C_c} = 1$, resulting in the exact group representation form eq (9).

D Group Convolution and Fourier Transform

D.1 Fourier transform on groups

The Fourier transform of a function $f : G \rightarrow \mathbb{R}$ at a representation $\varrho : G \rightarrow \text{GL}(d_\varrho, \mathbb{R})$ of G is

$$\hat{f}(\varrho) = \sum_{g \in G} f(g) \varrho(g). \quad (19)$$

For each representation ϱ of G , $\hat{f}(\varrho)$ is a $d_\varrho \times d_\varrho$ matrix, where d_ϱ is the degree of ϱ .

D.2 Dual group

Let \hat{G} be a complete set indexing the irreducible representations of G up to isomorphism, called the *dual group*, thus for each ξ we have an irreducible representation $\varrho_\xi : G \rightarrow U(V_\xi)$, and every irreducible representation is isomorphic to exactly one ϱ_ξ .

D.3 Inverse Fourier transform

The inverse Fourier transform at an element g of G is given by

$$f(g) = \frac{1}{|G|} \sum_{\xi \in \hat{G}} d_{\varrho_\xi} \text{Tr} \left[\varrho_\xi(g^{-1}) \hat{f}(\varrho_\xi) \right]. \quad (20)$$

where the summation goes over the complete set of irreps in \hat{G} .

D.4 Group Convolution

The convolution of two functions over a finite group $f, g : G \rightarrow \mathbb{R}$ is defined as

$$(f * h)(c) \equiv \sum_{b \in G} f(c \circ b^{-1}) h(b) \quad (21)$$

D.5 Fourier Transform of Group Convolution

Fourier transform of a convolution at any representation ϱ of G is given by the matrix multiplication

$$\widehat{f * h}(\varrho) = \hat{f}(\varrho) \hat{h}(\varrho). \quad (22)$$

In other words, in Fourier representation, the group convolution is simply implemented by the matrix multiplication.

Proof.

$$\widehat{f * h}(\varrho) \equiv \sum_c \varrho(c) \sum_b f(c \circ b^{-1}) h(b) \quad (23)$$

$$= \sum_c \varrho(c) \sum_{a,b} f(a) h(b) \delta_{(a, c \circ b^{-1})} \quad (24)$$

$$= \sum_{a,b} f(a) h(b) \sum_c \varrho(c) \delta_{(a \circ b, c)} \quad (25)$$

$$= \sum_{a,b} f(a) h(b) \varrho(a \circ b) \quad (26)$$

$$= \sum_a f(a) \varrho(a) \sum_b h(b) \varrho(b) \quad (27)$$

$$= \hat{f}(\varrho) \hat{h}(\varrho). \quad (28)$$

where δ is the Kronecker delta function, and the equivalence between $a = c \circ b^{-1}$ and $a \circ b = c$ is used between the second and the third equality. \square

E Group Convolution and Fourier Transform in HyperCube

HyperCube shares a close connection with group convolution and Fourier transform. On finite groups, the Fourier transform generalizes classical Fourier analysis to functions defined on the group: $f : G \rightarrow \mathbb{R}$. Instead of decomposing by frequency, it uses the group's irreducible representations $\{\varrho_\xi\}$, where ξ indexes the irreps (See Appendix D.2). A function's Fourier component at ξ is defined as:

$$\hat{f}_\xi \equiv \sum_{g \in G} f(g) \varrho_\xi(g). \quad (29)$$

Fourier Transform in HyperCube The Fourier transform perspective offers a new way to understand how HyperCube with a group representation eq (9) processes general input vectors. Consider a vector f representing a function, *i.e.*, $f_g = f(g)$. Contracting f with a model factor A (or B) yields:

$$\hat{f} \equiv f_g A_g = \sum_{g \in G} f(g) \varrho(g), \quad (30)$$

which calculates the Fourier transform of f using the regular representation ϱ . As ϱ contains all irreps of the group, \hat{f} holds the complete set of Fourier components. Conversely, contracting \hat{f} with ϱ^\dagger (*i.e.* factor C) performs the *inverse Fourier transform*:

$$\frac{1}{n} \text{Tr}[\hat{f} C_g] = \frac{1}{n} \sum_{g' \in G} f_{g'} \text{Tr}[\varrho(g') \varrho(g)^\dagger] = f_g, \quad (31)$$

where eq (2) is used. This reveals that the factor tensors generalize the discrete Fourier transform (DFT) matrix, allowing the model to map signals between the group space and its Fourier (frequency) space representations.

Through the lens of Fourier transform, we can understand how the model eq (10) processes general input vectors (f and h): it calculates their Fourier transforms (\hat{f} , \hat{h}), multiplies them in the Fourier domain ($\hat{f}\hat{h}$), and applies the inverse Fourier transform. Remarkably, this process is equivalent to performing group convolution ($f * h$). This is because the linearized group operation (Section 4.1) naturally entails group convolution (see Appendix E.1,E.2).

This connection reveals a profound discovery: HyperCube’s ability to learn symbolic operations is fundamentally the same as learning the core structure of group convolutions. This means HyperCube can automatically discover the essential architecture needed for equivariant networks, without the need to hand-design them. This finding highlights the broad potential of HyperCube’s inductive bias, extending its applicability beyond the realm of symbolic operations.

E.1 Reinterpreting HyperCube’s computation

HyperCube equipped with group representation eq (10) processes general input vectors f and h as

$$\begin{aligned}
 f_a h_b T_{abc} &= \frac{1}{n} \sum_a \sum_b f(a) h(b) \text{Tr} [\varrho(a) \varrho(b) \varrho(c)^\dagger] \\
 &= \frac{1}{n} \text{Tr} \left[\left(\sum_a \varrho(a) f(a) \right) \left(\sum_b \varrho(b) h(b) \right) \varrho(c)^\dagger \right] \\
 &= \frac{1}{n} \text{Tr} [(\hat{f}\hat{h}) \varrho(c)^\dagger] = \frac{1}{n} \text{Tr} [\widehat{f * h} \varrho(c)^\dagger] \\
 &= (f * h)_c.
 \end{aligned} \tag{32}$$

Therefore, the model calculates the Fourier transform of the inputs (\hat{f} and \hat{h}), multiplies them in the Fourier domain ($\hat{f}\hat{h}$), and applies the inverse Fourier transform, which is equivalent to the group convolution, as shown in Appendix D.5.

E.2 Group Convolution by D

Here we show that the linearized group operation \tilde{D} in Section 4.1 is equivalent to the group convolution in Appendix D.5.

Consider contracting the data tensor D with two functions $f, h \in G$, as

$$f_a h_b D_{abc} = \sum_{ab} f(a) h(b) \delta_{(a, cob^{-1})} = \sum_b f(c \circ b^{-1}) h(b) \equiv (f * h)(c), \tag{33}$$

which computes the group convolution between f and h , similar to eq (32). Here, we used $D_{abc} = \delta_{(aob, c)} = \delta_{(a, cob^{-1})}$.

F Supplemental Figures for Section 6

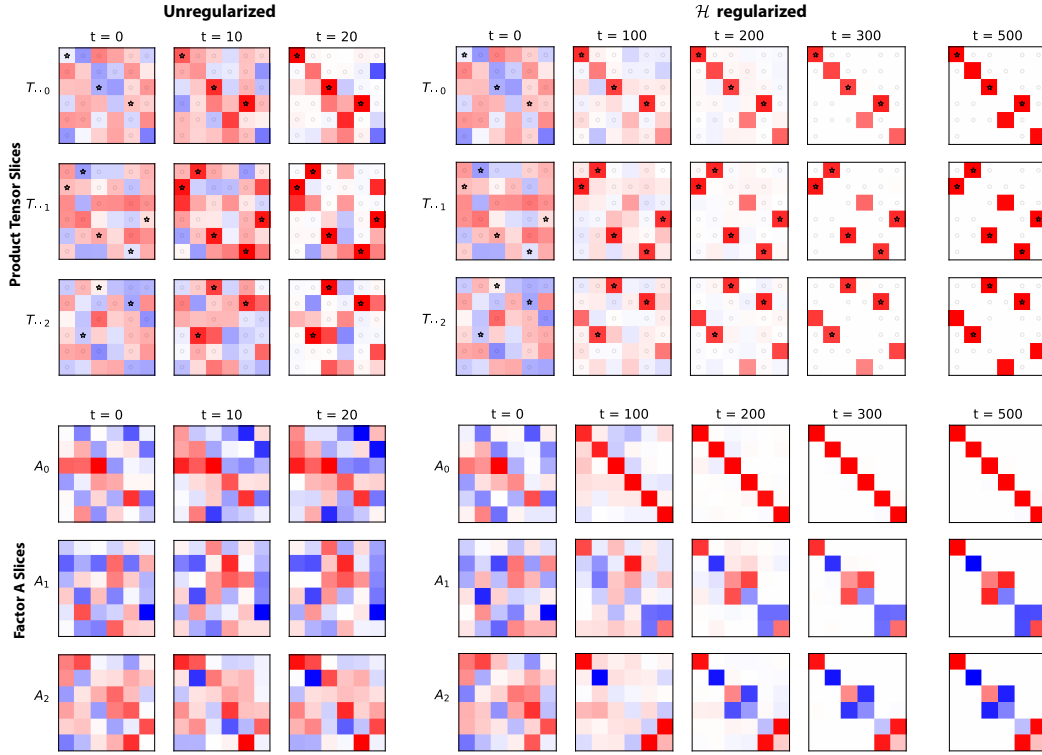


Figure 9: Visualization of the model T and factor A during training on the symmetric group S_3 (see Fig 4). (Top) Model slices: $T_{\cdot,c}$. The unregularized model quickly converges to a solution with poor generalization. The \mathcal{H} -regularized model converges to a generalizing solution around $t = 200$. It accurately recovers D when the regularization diminishes around $t = 400$ ($\epsilon \rightarrow 0$). (Bottom) Factor A slices: A_n . The unregularized model shows minimal changes from random initial values, while \mathcal{H} -regularized model shows significant internal restructuring. Shown in the block-diagonalizing coordinate. See Fig 10 (Bottom). Only the first three slices are shown. (color scheme: red=1, white=0, blue=-1.)

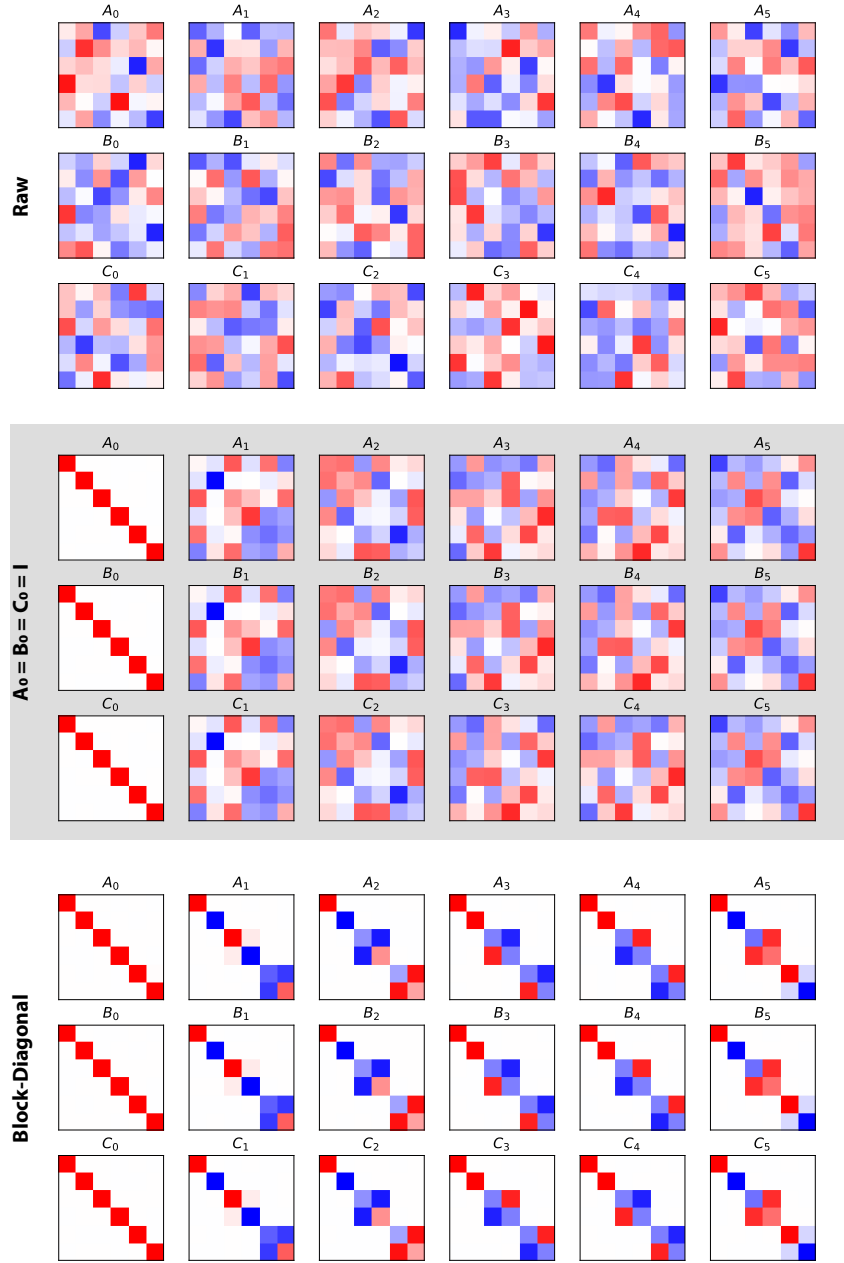


Figure 10: Learned factors of the \mathcal{H} regularized model trained on the S_3 group. (Top) Raw factor weights shown in their native coordinate representation. (Middle) Unitary basis change using $U_I = I$, $U_K = A_0$, $U_J = B_0^\dagger$, which yields $\hat{A}_0 = \hat{B}_0 = \hat{C}_0 = I$. (Bottom) Factors in a block-diagonalizing basis coordinate, revealing their decomposition into direct sum of irreducible representations. (color scheme: red=1, white=0, blue=-1.)

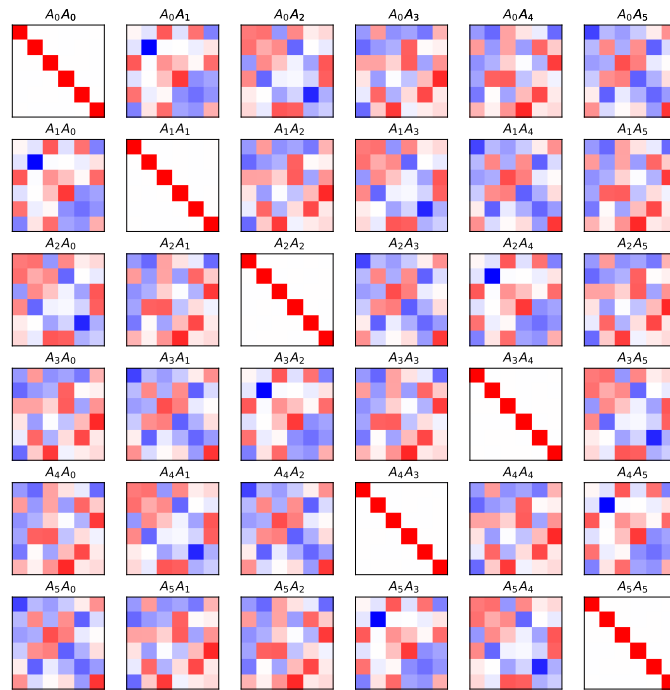


Figure 11: Multiplication table of matrix slices of factor A from the mid panel of Fig 10. Note that this table share the same structure as the Cayley table of the symmetric group S_3 in Fig 1. (color scheme: red=1, white=0, blue=-1.)

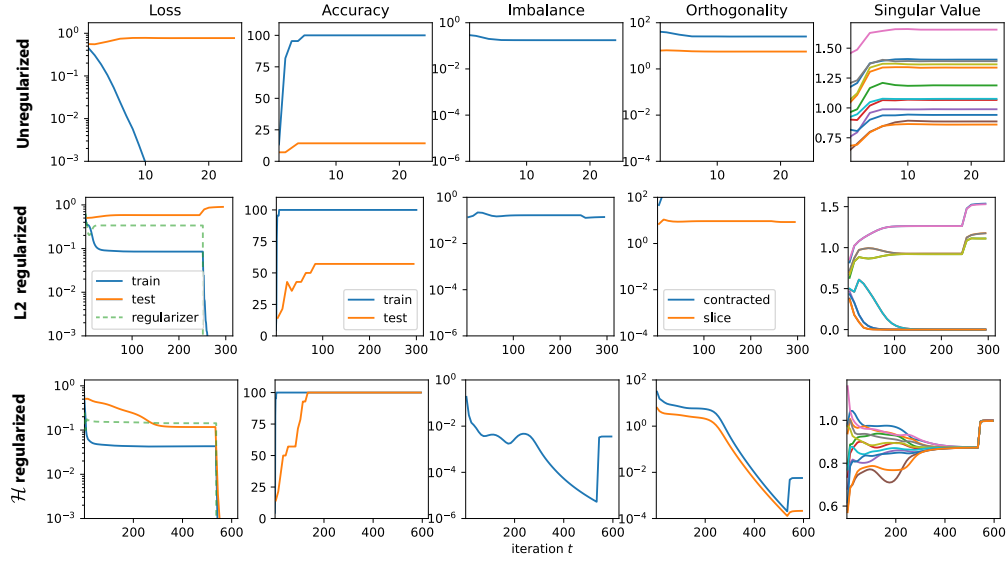


Figure 12: Optimization trajectories on the modular addition (cyclic group C_6) dataset, with 60% of the Cayley table used as train dataset (see Fig 13). (Top) Unregularized, (Middle) L2-regularized, and (Bottom) \mathcal{H} -regularized training.

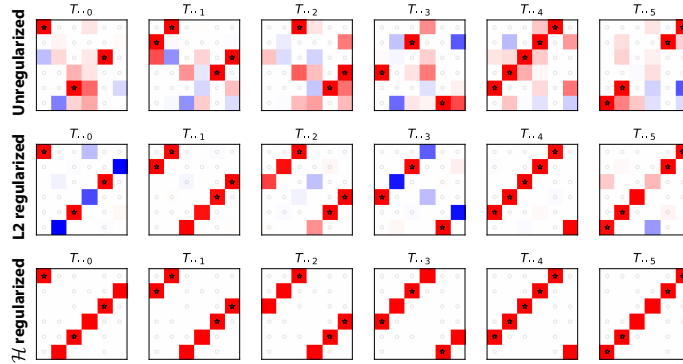


Figure 13: Visualization of product tensors after training on the modular addition (cyclic group C_6) under different regularization strategies (see Fig 12). The observed training data are marked by asterisks (1s) and gray circles (0s). Only the \mathcal{H} regularized model shows perfect recovery of the data tensor D . (color scheme: red=1, white=0, blue=-1.)

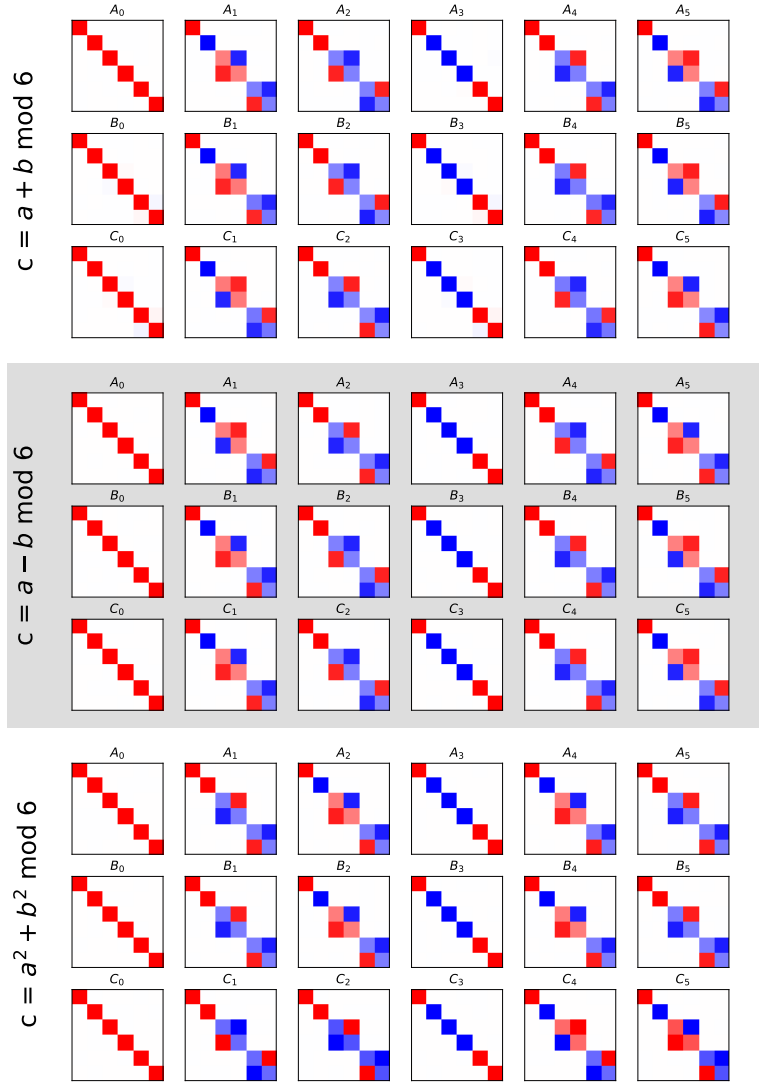


Figure 14: Visualization of factors trained on small Cayley tables from Figure 1. (Top) $c = a + b \bmod 6$, satisfying $A_g = B_g = C_g^\dagger = \varrho(g)$. (Middle) $c = a - b \bmod 6$, satisfying $A_g^\dagger = B_g = C_g = \varrho(g)$. (Bottom) $c = a^2 + b^2 \bmod 6$, which exhibits the same representation as modular addition for elements with unique inverses (e.g., $g = 0, 3$). For others, it learns *duplicate* representations reflecting the periodicity of squaring modulo 6: e.g., $A_2 = A_4$ and $A_1 = A_5$, since $2^2 = 4^2$ and $1^2 = 5^2$. (color scheme: red=1, white=0, blue=-1.)